Surface-State Enhancement of Tunneling Thermopower on the Ag(111) Surface

Petro Maksymovych,*,† Simon J. Kelly,† and Jorge I. Cerdá‡

†Center for Nanophase Materials Sciences, Oak Ridge National Laboratory, Oak Ridge, Tennessee 37831, United States and ‡Instituto de Ciencia de Materiales de Madrid, ICMM-CSIC, Cantoblanco, 28049 Madrid, Spain

ABSTRACT Thermoelectric effects in tunnel junctions are currently being revisited for their prospects in cooling and energy harvesting applications, and as sensitive probes of electron transport. Quantitative interpretation of these effects calls for advances in both theory and experiment, particularly with respect to the electron transmission probability across a tunnel barrier which encodes the energy dependence and the magnitude of tunneling thermopower. Using noble metal surfaces as clean model systems, we demonstrate a comparatively simple and quantitative approach where the transmission probability is directly measured experimentally. Importantly, we estimate not only thermovoltage, but also its energy and temperature dependencies. We have thus resolved surface-state enhancement of thermovoltage, which manifests as 10-fold enhancement of thermopower on terraces of the Ag(111) surface compared to single-atom step sites and surface-supported nanoparticles. To corroborate experimental analysis, the methodology was applied to the transmission probability obtained from first-principles calculations for the (111) surfaces of the three noble metals, finding good agreement between overall trends. Surface-state effects themselves point to a possibility of achieving competitive performance of all-metal tunnel junctions when compared to molecular junctions. At the same time, the approach presented here opens up possibilities to investigate the properties of nominally doped or gated thermoelectric tunnel junctions as well as temperature gradient in nanometer gaps.

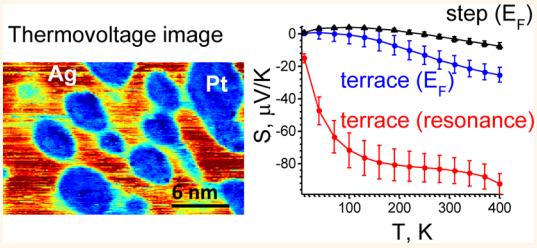

KEYWORDS: thermovoltage · tunneling · Landauer · resonance · thermopower · silver

Thermoelectric effects in tunnel junctions have recently regained significant interest in the context of transport through single molecules[1−4] and prospects for solid-state cooling.[5] Thermovoltage in tunnel junctions is also the basis for scanning thermovoltage microscopy, a technique based on scanning tunneling microscopy introduced by Williams and Wickramasinghe nearly three decades ago.[6] Scanning thermovoltage is capable of attaining chemical information[7,8] and enhancing the sensitivity of quasiparticle interference imaging,[9,10] both of which valuably complement more traditional tunneling spectroscopy.[11]

Although thermovoltage itself is relatively straightforward to measure in a nanoscale junction, establishing its relation to the transport properties of this junction is much more ambiguous. Revealing this relation is essential to make the relevant techniques quantitative and to chart deterministic pathways toward improvement of thermoelectric performance of nanojunctions. Within the context of scanning tunneling microscope (STM) experiments, the challenge of a quantitative interpretation of thermovoltage measurements is the relative difficulty of a quantitative analysis of the transport problem both experimentally and theoretically. This includes, of course, the normally unknown atomistic and electronic structure of the STM tip. Additional uncertainty lies in the temperature gradient across a nanojunction,[12,13] which will generally deviate from macroscopically measured ΔT and will introduce a systematic error into the estimation of the thermopower or Seebeck coefficient from the measured thermovoltage using $S_{th} = V_{th}/\Delta T_{macro}$.

At present, the interpretation of many experimental and theoretical works on thermovoltage in molecular junctions[14−16] relies largely on DFT-based calculations of

* Address correspondence to maksymovychp@ornl.gov.

Received for review May 21, 2014 and accepted November 18, 2014.

Published online November 18, 2014
10.1021/nn506123g

the transmission coefficient of the junction ($\sigma(\varepsilon)$). Thermopower is then estimated as

$$S_{th} = \frac{\pi^2 {k_B}^2 T}{3e}\left(\frac{d \ln\sigma(E)}{dE}\right)_{E_F} \quad (1)$$

analogous to the Mott formula for thermopower. Like the Mott formula, eq 1 is valid in the regime of linear response, weak energy dependence of the transmission coefficient $\sigma(\varepsilon)$, and cryogenic temperatures.[2,17] Though some of these conditions are perhaps valid for experiments, the biggest uncertainty in this case is reliance on the theoretical $\sigma(\varepsilon)$, which may strongly depend on the chosen method of calculation[18,19] and can be subject to its own errors.[20]

Scanning thermovoltage experiments are generally interpreted with the fundamentally similar approach[10,21−24] that was put forth by Stovneng and Lipavsky[25] (SL) in the early 1990s. The SL model also arrives at a Mott-like formula for a tunnel junction, but it does so by following the Tersoff−Hamann approximation for a tunnel junction under the assumption of a spherically symmetric (s-type) wave function at the tip. Under a further assumption of a WKB-like exponential dependence of the local density of states of the surface ($\rho_s(r,\varepsilon)$), the expression for the thermovoltage for a junction between the tip (at temperature T_T) and the surface (at temperature T_S) is

$$V_{th} = \frac{\pi^2 k_B^2 (T_T^2 - T_S^2)}{6e}\left(\frac{\partial \ln\rho_S(r_T,\varepsilon)}{\partial\varepsilon} + \frac{\partial \ln\rho_T(r_T,\varepsilon)}{\partial\varepsilon} + \frac{z}{\hbar}\sqrt{\frac{2m_0}{\varphi}}\right)_{E_F} \quad (2)$$

where m_0 is the free-electron mass and r_T is the geometric center of the tip-apex. The tunneling process contributes a linear term in z (tip−surface distance), which some of us have recently verified in STM experiments on a silver surface.[26] However, the material-specific parameters (first and second term in eq 2) are not readily accessible from the experiments. Although tunneling spectroscopy may directly measure the electronic density of states as $\rho_s \sim ((dI)/(dV))$, eqs 1 or 2 require, at the very least, to measure a second derivative of current $((d^2I)/(dV^2))$ to estimate $((\partial\rho)/(\partial\varepsilon))$ and from that the thermopower. This is not trivial to do accurately, given the typically high values of tunneling resistance, operating temperatures close to 300 K, and small signals. A number of papers applied eq 2 (or numerical integration of the more general Tersoff−Hamann-based expressions) to interpret the contrast arising from the standing waves of the surface-state electrons, addressing not only observed Friedel oscillations but also their spatial decay.[9,10,22] The respective models do indeed provide a very good match to experimental observations in a number of respects, primarily because the oscillatory component of the density of states in the vicinity of extended defects (due to Friedel oscillations) is well-defined. However, the absolute magnitude of the observed thermovoltage is not exactly reproduced.[10,22] The values for other surfaces where tunneling thermopower has been measured (such as silicon,[22] graphene[27]) also remain to be quantitatively understood.

Here we present a combined experiment−theory approach to interpret experiments on tunneling thermovoltage, which relies on the well-known Landauer formalism to remove some of the above-mentioned limitations and experimental uncertainties. We employ experimental tunneling spectroscopy data to directly estimate quantitative values of thermopower at any temperature. To illustrate its applicability, we characterized pure Ag(111) and Au(111) surfaces and the Ag(111) surface covered with metal particles. Outside of the methodological utility, the most interesting consequence of this analysis is a surprisingly large Seebeck coefficient of the Ag(111) terraces which we ascribed to the close proximity of the surface state band minimum to the Fermi level. In fact, our results reveal that all-metal junctions can be very competitive with the presently known molecular junctions with respect to thermopower, and they can likely be superior in terms of overall efficiency of thermoelectric energy conversion due to minimum achievable, though not negligible,[28] thermal coupling across the gap. Furthermore, since our approach still relies on a single-particle tunneling picture, its experimental consistency allows for a future search of interesting cases where many-body interactions of different nature could be identified and analyzed.

RESULTS AND DISCUSSION

Thermovoltage Measurements. Our general observation from all the experiments on the Ag(111) surface, including the bare surface and surface with metal nanoparticles, is that the thermovoltage signal is always largest on the surface terraces and in locations away from metal nanoparticles. This is seen in the thermovoltage images in Figures 1 where single-atoms steps, Pt nanoparticles, and Fe nanoparticles on the silver surface are always seen as regions of lower thermovoltage (Figure 1b,f). This overall contrast does not depend on the specific temperature of the measurement or even the physical tip and its termination. Lower values on single-atom steps[22] and copper nanoparticles on Ag(111)[7] were also previously reported.

From eq 2 the thermovoltage contrast stems from both surface-specific and tunneling terms, the latter scaling as $1/\sqrt{\phi}$, where ϕ is the barrier height. Both of these terms can and do contribute to the observed contrast.[22,26] Another potential but experimentally rather ambigious source of contrast in thermovoltage measurements is the local variation of the thermal gradient due to local changes of thermal coupling across the gap.[12,28] To ascertain the origin of the observed thermoelectronic contrast, we acquired

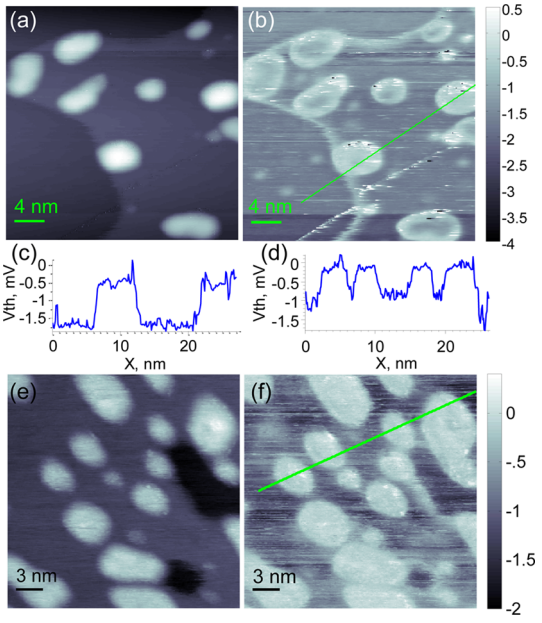

Figure 1. Scanning thermovoltage images of the Ag(111) surface with a small coverage of metal nanoparticles. (a) Constant conductance STM image and (b) corresponding thermovoltage image of Ag(111) with Fe nanoparticles; (e) constant conductance STM image and (f) corresponding thermovoltage image of Ag(111) surface with Pt nanoparticles; (c, d) line-profiles of thermovoltage signal across images in (b, f) correspondingly. Scale bars are in units of mV.

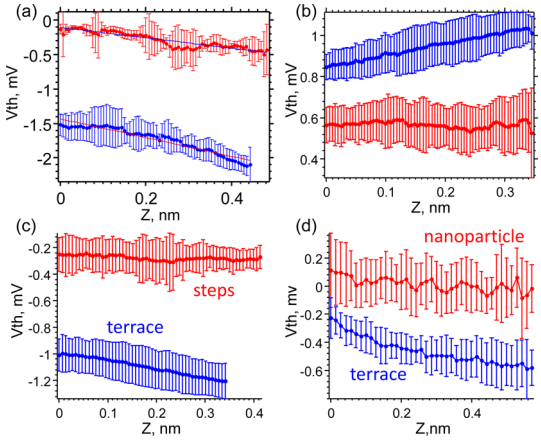

Figure 2. Distance dependence of tunneling thermovoltage. (a−c) Comparison of distance dependencies over steps and terraces obtained from three different measurements. Macroscopic sample temperature was set at 330.7 K in (a), 315 K (b), and 283 K (c), while the microscopic temperature of the tip of 298 K in all three measurements. (d) Comparison of the Ag(111) terrace and Pt nanoparticles. The surface temperature was ∼340 K. The data presents averages of 10−50 individual distance-dependent spectra of tunneling thermovoltage.

distance-dependence of thermovoltage over the terraces, steps and nanoparticles.[26] The corresponding data are shown in Figure 2. We observe that despite large differences in the absolute magnitude of the thermovoltage, the slopes of V_{th} vs tip−surface distance are approximately similar in all cases. This signifies that the observed contrast is not arising primarily from the vacuum-term, or the differences in the barrier height (at least to within the measured accuracy). The similarity of the slopes further suggests that the differences are relatively minor in the local temperature gradient.[26] Alternatively, if indeed either the temperature gradient or vacuum terms dominated the observed contrast in thermovoltage, the respective $V_{th}(z)$ dependencies would cross (or almost cross) at the assumed $z = 0$ point (see eq 2). As seen in Figure 2, the $V_{th}(z)$ dependencies measured over the atomic steps and terrace may indeed cross. However, the extrapolated crossing point is −2.1 nm and −1.3 nm for Figure 2a and Figure 2c, correspondingly. This is much too large to be compatible with the width of the tunnel junction. The situation is less clear in Figure 2b, although given the magnitude of the error bars we do not believe the difference here can be solely due to the vacuum terms.

Because of the significant slope of $V_{th}(z)$, quoting one specific value for the thermopower of the junction is unjustified. Using the minimum-observed values however and assuming that ΔT drops solely across the junction, we obtain values of −40 μV/K for the terrace and −3 μV/K for the step in Figure 2a, −85 μV/K for the terrace and −56 μV/K for the step in Figure 2b, and −44.5 μV/K for the terrace and −11 μV/K for the step in Figure 2c. Although the individual values scatter significantly, the *difference* in S_{th} between the steps and the surface is much more consistent, being −37, −29, and −33 μV/K for Figure 2a−c, correspondingly. These values are consistent with a previous measurement of −45 μV/K.[7] Notably, the values for the terraces by themselves are at least an order of magnitude larger than what is expected for bulk silver.[29] Since the step sites have a lower work-function, according to eq 2 the thermopower should be *larger* at the steps than at the terraces, opposite to the experimental trend. The contribution, however, is small; a difference of ∼0.5 eV in the work-function would amount to only 0.5−3.5 μV/K at 300 K. The order of magnitude larger difference observed experimentally *must* therefore be intrinsic to the surface and related to the differences in the electronic structure.

Systematic analysis of the differences between various clusters and topographic features on a surface requires, of course, the knowledge of their electronic structure. To simplify the problem and obtain a good quantitative reference for theoretical calculations, we also compared thermovoltage of bare Ag(111) and Au(111) surfaces measured with the same physical tip (Figure 3). As seen in Figure 3a,b, thermovoltage on Ag(111) is about a factor of 5 larger than that on the terraces of Au(111) (Figure 3c−e), a remarkably large contrast. Both thermovoltage images appear "streaky" along the short scan axis due to inevitable and continuous modification of the tip apex at room

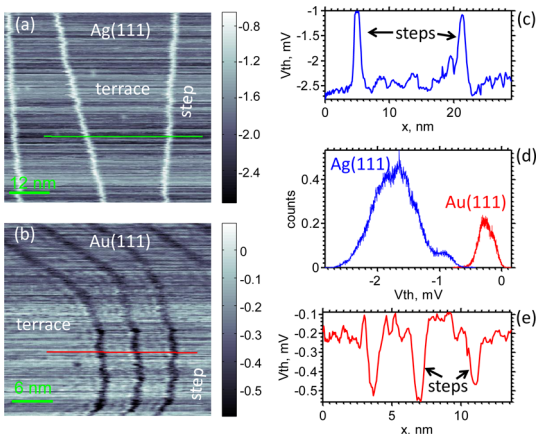

Figure 3. Direct comparison of thermovoltage on Ag(111) and Au(111) surfaces obtained with the *same physical tip*. (a, b) Thermovoltage images of clean Ag(111) and Au(111) surfaces, in each case showing distinct contrast due to single atom steps. Note that the step-terrace contrast is reversed between Ag(111) and Au(111) surfaces. (c) Line profile of thermovoltage across Ag(111) surface. (d) Comparison of thermovoltage histograms obtained from images (a) and (b). (e) Line-profile of the thermovoltage across Au(111) surface. Temperature of the surface was stabilized at 340 K during the measurements. The bulk of the STM tip is at 298 K.

temperature (which effectively results in large thermovoltage noise). This, in particular, results in a very broad distribution of thermovoltage values (with a net width up to 0.8 mV). The relative mean value of the thermopower of the Ag(111) surface ($\langle S_{Ag(111)}\rangle = (\langle V_{surf}\rangle - \langle V_{step}\rangle)/\Delta T$) equals $\sim -20\ \mu$V/K, a lower estimate due to broadening. From the line-profile (which corresponds to approximately the same tip condition for all the values) in Figure 3c we obtain $\sim -32.6\ \mu$V/K, in excellent agreement with the point spectra in Figure 2. For Au(111) terraces, a similar estimate gives a value of $-4.7\ \mu$V/K.

Also note that on Au(111) the thermopower of the steps is larger by a factor of 2 ($\sim -12\ \mu$V/K, Figure 3e) compared to its terraces. As a result, the step-terrace thermovoltage contrast is inverted between Ag(111) and Au(111) surface. As we will show in the following, the reason for this difference is that the effect of the surface state is almost negligible on Au(111), although steps do suppress the surface state band on both surfaces. However, the fact that steps themselves appear to have significant thermopower in their own right and that steps on Ag(111) and Au(111) surface have approximately 2-fold difference in thermovoltage (Figure 3c vs Figure 3e) is quite noteworthy and has to be rooted in the localized electronic structure of the step sites.

High-quality tunneling thermovoltage measurements by other groups also showed almost negligible values of thermovoltage on the Au(111) surface on the terraces far away from single atoms or steps. In the vicinity of the steps thermovoltage shows oscillatory behavior due to screening of the step-potential by the surface state and the resulting Friedel oscillations of electron density (they can be seen in Figure 3b). In this case, there is an added energy-dependent component of the surface state density that will contribute to thermovoltage.[9,22]

Theoretical Calculations of Thermopower. Prior to presenting our S_{th} estimations both theoretically and employing experimental d*I*/d*V* spectra, we revisit the most common approximations employed for the estimation of S_{th} in tunnel junctions paying attention to their adequacy for being employed in conjunction with experimental data. Assuming the substrate and tip are in chemical and thermal equilibrium with their respective reservoirs with chemical potentials μ_s and μ_t and temperatues T_S and T_T, respectively, the thermovoltage V_{th} is defined from the condition

$$I_{th}(V = 0, T_S, T_T) + I_{th}(V_{th}, T, T) = 0 \qquad (3)$$

where I_{th} is the thermal current at zero bias and I is the *electronic* current evaluated at $T = 1/2(T_S + T_T)$ under a bias of $V_{th} = (\mu_T - \mu_S)/e$. Here we follow the usual STM convention whereby positive bias implies a net current from the tip to the sample (empty states at the surface). The thermopower or Seebeck coefficient, S_{th}, is then given by

$$S_{th} = -\lim_{\Delta T \to 0} \frac{V_{th}}{\Delta T} \qquad (4)$$

with $\Delta T = T_T - T_S$.

A general single-particle expression for the current is provided by the Landauer formalism as

$$I(V, T_S, T_T) = \int_{-\infty}^{\infty} d\varepsilon \sigma(\varepsilon) \left[f_{FD}\left(\frac{\varepsilon - \mu_S + eV/2}{k_B T_S}\right) - f_{FD}\left(\frac{\varepsilon - \mu_T - eV/2}{k_B T_T}\right)\right] \qquad (5)$$

where $\sigma(\varepsilon)$ is the transmission coefficient (or differential current) and f_{FD} stands for the Fermi–Dirac distribution. If no approximations are made in eq 5, V_{th} needs to be solved numerically by finding the voltage at which the electric and thermal currents cancel out (condition given by eq 3). However, and given that thermovoltages attain very small values (of the order of 0.1 mV or lower), it is common to linearize the electric current as $I(V_{th}, T, T) = \sigma(\mu)V_{th}$, with $\mu = 1/2(\mu_S + \mu_T)$, to obtain an explicit expression for the thermopower:

$$S_{th} = \frac{I_{th}(V = 0, T_S, T_T)}{\sigma(\mu)\Delta T} \qquad (6)$$

The linear assumption should be valid as long as $\sigma(\varepsilon)$ remains constant within a $\sim[-k_BT, k_BT]$ interval around μ.

The well-known Landauer expression for single-particle thermopower is obtained by expanding Fermi–Dirac distribution functions around μ and T[17,30,31]

$$S_{th}(T,\mu) = \frac{1}{eT}\frac{\int_{-\infty}^{\infty} d\varepsilon(\varepsilon-\mu)\sigma(\varepsilon)\left[f'_{FD}\left(\frac{\varepsilon-\mu}{k_BT}\right)\right]}{\int_{-\infty}^{\infty}\sigma(\varepsilon)\left[f'_{FD}\left(\frac{\varepsilon-\mu}{k_BT}\right)\right]d\varepsilon} \quad (7)$$

where

$$f'_{FD}\left(\frac{\varepsilon-\mu}{k_BT}\right)$$

stands for

$$\partial f'_{FD}\left(\frac{\varepsilon-\mu}{k_BT}\right)/\partial\varepsilon$$

All our numerical tests show hardly any differences between approximations 6 and 7, both yielding essentially the same thermovoltages as the exact result derived from eqs 4 and 5. However, as discussed in the following, eq 7 is particularly well-suited for analysis of expeirmental data.

Stovneng and Lipavsky, in their analysis of thermovoltage in tunnel junctions, applied Sommerfeld-like expansion to eq 5, approximating thermoelectric current as[25]

$$I(V=0,T_S,T_T) \sim \frac{\pi^2 k_B^2}{6}(T_S^2 - T_T^2)\sigma'(\mu) \quad (8)$$

which then leads to the Mott-like expression for the thermopower

$$S_{th} = \frac{\pi^2 k_B^2}{3e} T[\ln\sigma(\mu)]' \quad (9)$$

which predicts a linear dependence of S_{th} with temperature. Notice that eq 9 can also be obtained from eq 7 in the limit of $T = 0$, where

$$f'_{FD}\left(\frac{\varepsilon-\mu}{k_BT}\right) \to \delta(\varepsilon-\mu)$$

Lunde and Flensberg[17] studied the range of validity of the SL approach eq 9 *versus* Mott's approximation (where the temperature is included in the conductance, $\sigma(\mu) = \sigma(\mu,T)$ to find that the latter works better at high temperatures. In the next section we will also examine the accuracy of these approaches focusing on the range of variation of $\sigma(\varepsilon)$ around μ.

In order to address the origin of the large thermopower values found at the Ag(111) terraces compared to Au(111) terraces, we have performed a comparative study for the clean (111) surfaces of the noble metals following the *ab initio* formalism described above. In Figure 4a, we present the calculated surface state (SS) band dispersion for the Cu, Ag, and Au(111) surfaces. The onsets of the SS bands are −434, −80, and −354 meV, respectively, in fair agreement with experimental reported values of −435, −63, and −484 meV.[32] We next calculated the transmission coefficients, $\sigma(\varepsilon)$, across an STM setup by placing a semi-infinite tip block at several heights ($z = 4-8$ Å) from the surface. For each case the tip was assumed of the same element as the surface with a sharp one-atom ended apex. We adopt this choice because the experimental tips were always prepared by soft contact with the metal and, therefore, we expect the apex to end up covered with the same material as that at the surface. For the Ag case we additionally considered a more blunt three-atom terminated apex. Figure 4b shows the resulting differential currents normalized to the conductance, $\sigma(\varepsilon)/\sigma(\mu)$, for the three metals and a tip height of $z = 5$ Å. All curves reproduce the step at the onset of the SS well. The bulk background shows a slight positive slope which increases with z (data not shown).

Seebeck coefficients, S_{th}, calculated for the three surfaces are displayed in Figure 4c as a function of temperature $T = 0.5(T_S + T_T)$ and three different tip heights. In order to test the validity of the different theoretical approximations, we plot with solid lines the values obtained with the most general approach eqs 4 and 5), with dotted lines those obtained after linearizing the electrical current (eq 6), and with dashed and dashed-dotted lines the SL and Landauer formulas (eqs 9 and 7, respectively). The four approaches yield very similar thermopowers for Cu and Au, with an almost perfect linear dependence with temperature and small negative values of just a few $\mu V/K$. The slopes in both metals attain negative values and increase in absolute value as the tip is retracted. Only for Au at the closest tip−sample distance of $z = 4$ Å is the sign of the slope inverted, and the thermopower attains positive values.

The case of silver, however, is quite different; S_{th} deviates considerably from linearity showing a curvature that yields Seebeck coefficients of up to $-10\,\mu$V/K at RT, that is, almost 1 order of magnitude larger than for Cu or Au. Calculations predict approximately 5-fold enhancement of thermopower on Ag(111) relative to Au(111) surface, in very good agreement with the experimental data in Figure 3. We have additionally checked that the thermopower does not depend on the precise location of the tip after placing the apex end atom on top of a surface 3-fold site to find that the normalized conductance is indistinguishable from the atop case, which is an expected result given the large spatial delocalization of the SS.

In the case of Ag(111), the SL approach deviates substantially from the rest already at 150 K, while the Landauer expression yields results indistinguishable from the exact ones (solid lines superimposed on the dashed-dotted lines). The linearization approach of eq 6, on the other hand, is not as accurate as it presents small deviations at high temperatures. The reason for enhancement of S_{th} and the failure of the SL theory in the case of silver is obviously the far from smooth $\sigma(\varepsilon)$ behavior around μ due to the proximity of the SS, which shoots the $[[\ln\sigma(\mu)]'$ term in eq 9 making further terms in the Sommerfeld expansion involving higher order

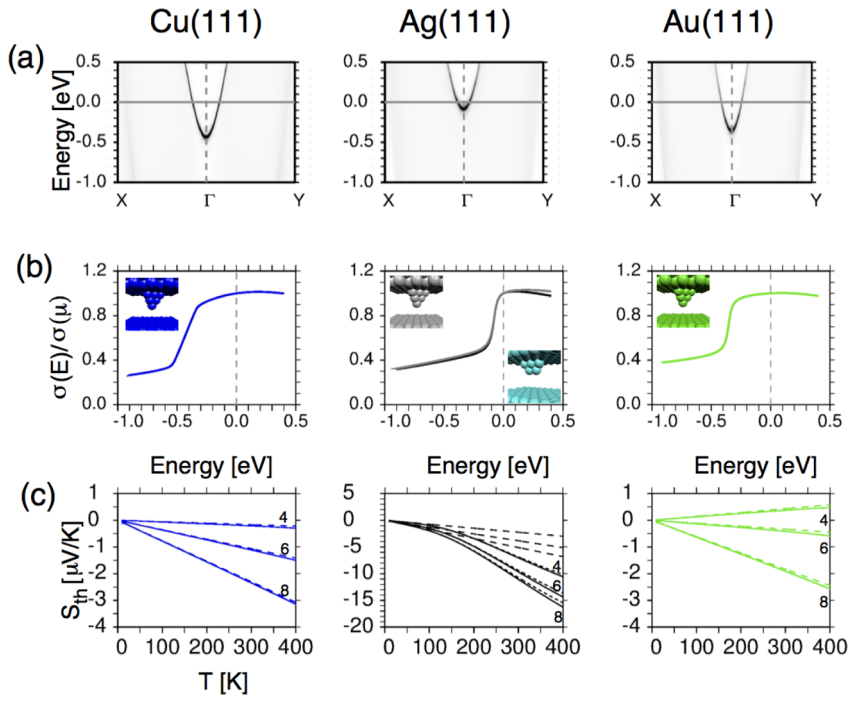

Figure 4. Theoretical analysis of tunnel junctions. (a) k-resolved DOS projected on the surface layer of the semi-infinite Cu(111), Ag(111), and Au(111) surfaces. (b) Normalized transmission coefficient, $\sigma(\varepsilon)/\sigma(\mu)$, for the Cu(111) + Cu-tip, Ag(111) + Ag-tip, and Au(111) + Au-tip systems. For the Ag case (middle column), results for two different tips are shown: sharp one-atom ended apex (dark line) and a *blunt* 3-atom ended apex (gray). (c) Thermopower as a function of temperature *T* for the three surfaces and three different tip heights, z_{tip}, indicated in angstroms close the each solid line. Solid lines correspond to the general approach of eqs 4 and 5, dotted lines after linearizing the current *via* eq 6, dashed lines to the SL formula 9 and dashed-dotted to the Landauer expression 7, although they are not visible due to perfect match with the solid lines. See text for further explanations.

derivatives necessary. Indeed, if we artificially place the chemical potential precisely at the SS location, even larger Seebeck coefficients of around -25 μV/K can be obtained. The theoretical analysis therefore, confirms that the proximity of the SS band onset to the Fermi level is the main factor responsible for the large thermopower measured on the Ag(111) terraces.

Calculation of Thermopower Based on Tunneling Spectroscopy. Experimental analysis should not be limited to relative contrast of thermovoltage. In the following, we discuss how cryogenic tunneling spectroscopy can be used to estimate both high temperature values of thermopower and its actual temperature-dependence. The Landauer expression 7 is the best suited for an experimental approach to the thermopower. It is essentially exact and does not include any $[[\sigma(\varepsilon)]']$ terms which would require measuring the second derivative of current, $(d^2I)/(dV^2)$, a challenging task particularly at elevated temperatures. Still, the experimental application of eq 7 in order to recover $S_{th}(\mu,V)$ is complicated due the lack of direct measurement of $\sigma(\varepsilon)$. However, at cryogenic temperatures, such that $\partial f(\varepsilon-\mu)/\partial\varepsilon \cong \delta(\varepsilon-\mu)$, tunneling spectroscopy becomes a direct measurement of the differential current, $dI/dV = G = ((e^2)/(\pi\hbar))\sigma(\varepsilon))$, provided it is more or less free from instrumental artifacts (most notable is that the modulation techniques used to acquire the first derivative of current, dI/dV, are conditioned to as small instrumental broadening as possible, or the effect of the broadening are accounted for systematically).

Figure 5a compares tunneling spectra acquired over a clean terrace on the Ag(111) surface and over single atom steps. The statistics was derived from at least 30 spectra acquired on a grid of surface positions, while the spectra were acquired with a lock-in amplifier and a minimal oscillation amplitude of 1−2 mV. Though any STM tip can detect the surface state, the exact shape and intensity of the resonance varies rather significantly, as is seen from the difference in the shape of the two blue lines in Figure 5a. The surface state is quenched at the step (red line), significantly increasing the measured conductance of the step-site below -60 mV. We do, however, observe a small peak at the Fermi level, which could originate from the tip state.

Upon inserting these spectra into eq 7, one may analyze the thermopower as a function of temperature. In Figure 5b, we present the resulting temperature dependence of S_{th}. Thermopower at 330 K extracted from a variety of data sets falls into the range of -19 ± 5 μV/K and -2.6 ± 2 μV/K at the terraces and steps, correspondingly. These values agree reasonably well with those obtained from direct thermovoltage measurements shown in Figure 2, although the value for

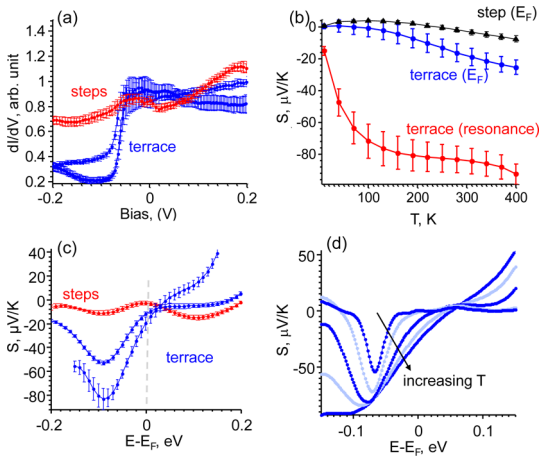

Figure 5. (a) Average tunneling spectra of the Ag(111) terrace and single-atom steps acquired at 4.5K (with tip and sample in thermal equilibrium). The data is the amplitude signal from the lock-in amplifier (oscillation amplitude 1.5 mV at 750 Hz). (b) Temperature-dependence of thermopower at the step evaluated at the true chemical potential (μ) vs that of the terrace at μ (blue) and for its minimum value close to the energy of the surface state band minimum (red). (c) μ-dependence of thermopower at 300 K calculated from (a) using eq 7. (d) μ-dependence of thermopower over the terrace for five different temperatures, 50, 100, 200, 300, and 400 K progressively increasing along the direction of the black arrow.

the terrace is systematically lower by at most a factor of 2. The possible sources of disparity are (1) instrumental broadening of the STS spectra in Figure 5a, which decreases the STS-extracted value of thermopower; (2) vacuum component of thermovoltage, which increases the directly measured value and is still influential given the small overall magnitude of thermovoltage; (3) sensitivity to subtle changes of the tip states, because thermopower is roughly proportional to the derivative of the DOS. Tip effects in particular, may easily explain why the absolute values of thermopower from Figure 2a−c are not as consistent as the relative difference between the step and the terrace. Furthermore, the very large value of thermovoltage on the step, measured in Figure 2 probably indicates that it is entirely tip-state dominated. As a corollary, focusing on relative rather than absolute values using some reference object on the surface is probably a better approach to quantitative interpretation of tunneling thermovoltage measurements.

The projected data in Figure 5b also shows a nice qualitative agreement with the theoretical temperature dependence of thermopower displayed in Figure 4c. In particular, negative values are obtained for the entire temperature range and deviation from linear behavior can be inferred above 100 K. This is not surprising given the good correspondence between the $\sigma(\varepsilon)$ curves in Figures 4b and 5a. However, we should note that the theoretical S_{th} values are consistently around a factor two smaller than the projected ones. The reason can be ascribed to the underestimation of the relative height of the surface state step with respect to the bulk background in Figure 4b, since it is roughly half the value measured by cryogenic STS. We are not certain for the reason for this discrepancy as it may be related to any of the various approximations employed in our theoretical formalism or to the actual tip shape. In this sense, and despite both a one- and three-atom ended apex yielding very similar $\sigma(\varepsilon)$ curves, experimental tips providing good resolution in STS data are generally believed to be much more flat (large radius of curvature). A more detailed comparison of theoretical and experimental transmission coefficient will be published elsewhere.

Another highly interesting aspect of eq 7 is that it allows to study the dependence of the Seebeck coefficient on the chemical potential (varying μ is nominally equivalent to band-filling or classical doping, though its detailed interpretation should be taken with care). In Figure 5c, we present the projected $S_{th}(\delta\mu)$ curves evaluated at RT after employing the spectra in Figure 5a. The SS band introduces a pronounced dip in thermopower, the magnitude of which can be as large as -90 μV/K, at the energy of SS onset. On the contrary, thermopower has an almost negligible energy dependence at the steps. Temperature dependence of thermopower at the terrace is manifested as a gradual broadening of the surface state derived dip, Figure 5d. This process will gradually increase the corresponding values both on resonance and at the Fermi level E_F (Figure 5d). Although the measured values should be approximately linear with temperature, below 100 K the magnitude drops to near-zero values.

CONCLUSIONS

We have performed a thermovoltage study of the Ag(111) surface following different perspectives: (i) directly acquiring thermovoltage scans at terraces, steps, and adsorbed metallic nanoparticles, (ii) performing *ab initio* calculations for the conductance, $\sigma(\varepsilon)$, across an STM junction comprising a defect-free surface and a sharp tip apex, and from that applying the Landauer formalism to extract the thermopower *via* eq 7 and (iii) same as (ii) but employing cryogenic STS data instead to obtain $\sigma(\varepsilon)$. As our main result we have found that the Ag(111) terraces present large thermopower values, up to one order of magnitude larger than those found at the steps, the adsorbed nanoparticles or other noble metal surfaces. The explanation becomes rather straightforward after taking into account the step in the conductance at the onset of the surface-state band and its proximity to the Fermi level. Quenching of the surface state band by the step, adsorbates, and nanoparticles due to local changes of lattice symmetry, band-folding, and chemical bonding will eliminate the strong resonance in $\sigma(\varepsilon)$ and reduce the overall magnitude of thermopower. The

physical picture is that the surface state band makes the probability of electron and hole transport across the barrier asymmetric around Fermi level, and this asymmetry (equivalent to particle hole asymmetry in conductors) is strongly reduced in its absence.

We need to stress that temperature and energy dependence of thermopower projected from cryogenic STS data applies to the junctions used to acquire the STS data and measures only the DOS contribution to thermopower. The effects of carrier-diffusion, electron−phonon, and electron−electron interactions cannot be captured by this method because there is no thermal gradient in the measured leads. Although this may be considered a weakness, a "clean" separation of the DOS effects from other contributions of thermopower can be a potent method to look for alternative strategies to enhance thermoelectric performance, including DOS engineering,[33,34] magnetic degrees of freedom,[35,36] and dimensionality effects.[37]

Finally, we note that surface-state enhancement similar to that observed on Ag(111) can make tunnel junctions very competitive if not superior to other tunnel junctions so far considered as candidates for thermoelectronic applications. Most notably, at present a large number of single molecule junctions[4,16,42] and single atom junctions[30] have been measured and predicted.[15,18] For the most part, the magnitude of thermopower rarely exceeds 50 μV/K in molecular junctions, but much smaller values around 5−20 μV/K are more common[16,31] and are also characteristic of atomic junctions.[30,39] Though Ag(111) by itself has a thermopower of −10 to −20 μV/K, changing the chemical potential to bring it closer to the SS onset can produce a value up to −100 μV/K (Figure 5d), which would be one of the highest values reported for local junctions. To shift the surface state one can invoke dielectric barriers,[40] such as a thin oxide or molecular film. More generally resonances at the Fermi level can be introduced with all-metal quantum wells, where the position and possibly width of the resonance can be designed on demand through an appropriate choice of the elements constituting the quantum well-junction and the thickness of the metal layers.[41] Linear increase of thermopower will translate into quadratic growth of ZT. Moreover, vacuum junctions have the smallest possible thermal conductivity. Its value for molecular junctions is still unknown, but it will be significantly higher nonetheless. Therefore, correctly engineered vacuum junctions can be an interesting candidate for elements with improved overall thermoelectric performance.

METHODS

Experimental Methods. A Ag(111) surface was prepared in ultrahigh vacuum using standard procedures of Ar^+ sputtering and postannealing to 700 K. Metals (Pt and Fe) were deposited from an e-beam evaporator onto a surface held at room temperature. The surface was postannealed to no more than 420 K after evaporation. Thermovoltage experiments were carried out using a variable temperature scanning tunneling microscope (derived from Omicron VT-SPM) following the procedure described previously.[26] Briefly, the temperature gradient was established by either cooling or heating the sample surface to the tip (assumed to be at 294 K). Thermovoltage was measured by nullifying thermoelectric current at zero applied bias using a PID controller. For imaging the thermoelectric signal, the STM feedback was switched from a constant current (I_T = const) to a constant conductance (dI_T/dV = const) mode, where a small AC voltage (2−3 mV, 800−900 kHz) applied to the tunneling gap was used to measure dI_T/dV. Distance-dependent thermovoltage spectroscopy was carried out with the PID controller (and AC amplitude nullified) or simply by acquiring I−V curves in the vicinity of zero bias as a function of tip−surface distance. The comparison between the Ag(111) and Au(111) surfaces was carried out with the same physical tip, within less than 1 h interval separating the measurements (to allow for thermal equilibration of separate sample holders). Spatial resolution of thermovoltage achieved in this paper is ∼1 nm, at least partly due to the relative bluntness of the STM tip. Cryogenic tunneling spectroscopy was acquired in a low-temperature scanning tunneling microscope (SPECS JT-STM) at 4.5K with the parameters specified in the text.

Theoretical Methods. All the calculations have been performed with the GREEN code[42] and its interface to the DFT-based SIESTA package.[43] The calculation of the transmission coefficient, $\sigma(\varepsilon)$, across an STM setup is treated with open boundary conditions and requires first a series of self-consistent calculations for different parts of the system as explained in detail in ref 44. We explored the (111) surface of the noble metals Cu, Ag, and Au *via* (1 × 1) 10 layers thick slabs. The tip apex for each element was modeled *via* (4 × 4) slabs comprising 9 bulk layers plus a sharp 10 atom pyramid stacked below (see insets in Figure 4b). For the Ag case, we additionally considered a *blunt* tip after removing the end atom at the apex. Finally, in order to address the tip−sample combined system we generated (4 × 4) 10 layers thick slabs placing the surface at the top of the slab and the apex at the bottom. The size of the supercell along the slab normal was varied in order to consider different tip−sample distances.[44] The self-consistent Hamiltonians for all the slab and bulk cells were computed within the SIESTA formalism and under the generalized gradient approximation (GGA) for the exchange-correlation energy.[45] For the generation of the numerical atomic orbitals employed by SIESTA as basis set we defined a double-ζ polarized scheme and set confinement energies of 100 meV for all atoms except those close to the vacuum region (first two surface layers in the surface slabs and all apex atoms in the tip slabs) for which highly extended orbitals were defined after setting the confinement energy to 10 meV. Real space meshes with a resolution of ∼0.07 Å^3 were employed for the numerical integration of three-center integrals, while Brillouin zones (BZs) were sampled with (15 × 15) *k*-grids. The first three interlayer spacings at the surfaces and all apex atoms in the tip slabs were allowed to relax until atomic forces were smaller than 0.01 Å/eV, with the rest of atoms fixed to bulk positions.

Once the Hamiltonians for each block were computed and stored, we calculated the Green's functions (GFs) and scattering states for a semi-infinite surface after matching the bulk and surface slabs *via* GF techniques.[44] Our calculation scheme allows to easily extract the density of states projected (PDOS) on the surface layer along high symmetry lines in the BZ and hence, obtain the surface state band dispersion superimposed on the bulk continuum of states (see Figure 4a). Semi-infinite blocks for the tips together with their scattering states were generated in a similar way, although the apex is considered as isolated after removing the interactions with its replicas in the (4 × 4) slab calculation and allowing mixing of all tip k-points

(*i.e.*, the BZ at the apex is shrinked to the Gamma point). The elastic transmission coefficient, $\sigma(\varepsilon,V)$, was then evaluated for each tip−sample distance calculating the GF of the entire system up to first order in the tip−sample interactions, which is equivalent to consider just one tunneling process (this approximation is highly accurate in the tunneling regime). On the other hand, and since we are primarily interested on the surface states, we employed a wide band limit (WBL) at the tip by fixing its DOS(ε) to that calculated at the Fermi level, μ. If we further assume that under an applied bias V all the potential drops in the vacuum region the transmission coefficient will only depend on the energy at the sample, $\sigma(\varepsilon,V) = \sigma(\varepsilon)$, and we may drop the V dependence in the transmission coefficient. For the electronic transport calculations we employed imaginary parts of the energy entering the GFs of 100 meV for the bulk and just 5 meV at the surface layer in order to obtain a good resolution. Accordingly, and given the high dispersive character of the metal bands around μ, the BZ sampling at the surface had to be increased considerably employing up to (256 × 256) k-grids to achieve a smooth $\sigma(\varepsilon)$ curve.

Conflict of Interest: The authors declare no competing financial interest.

Acknowledgment. A portion of this research (S.K.) was sponsored by the Laboratory Directed Research and Development Program of Oak Ridge National Laboratory, managed by UT-Battelle, LLC, for the U.S. Department of Energy. A portion of this research (P.M.) was conducted at the Center for Nanophase Materials Sciences, which is sponsored at Oak Ridge National Laboratory by the Scientific User Facilities Division, U.S. Department of Energy. J.I.C. acknowledges financial support from the Spanish Ministerio de Economía y Competitividad (Grant Nos. MAT2010-18432 and MAT2013-47878-C2-R).

REFERENCES AND NOTES

1. Aradhya, S. V.; Venkataraman, L. Single-Molecule Junctions Beyond Electronic Transport. *Nat. Nanotechnol.* **2013**, *8*, 399–410.
2. Dubi, Y.; Di Ventra, M. Colloquium: Heat Flow and Thermoelectricity in Atomic and Molecular Junctions. *Rev. Mod. Phys.* **2011**, *83*, 131–155.
3. Murphy, P.; Mukerjee, S.; Moore, J. Optimal Thermoelectric Figure of Merit of a Molecular Junction. *Phys. Rev. B* **2008**, *78*.
4. Reddy, P.; Jang, S.-Y.; Segalman, R. A.; Majumdar, A. Thermoelectricity in Molecular Junctions. *Science* **2007**, *315*, 1568–1571.
5. Edwards, H. L.; Niu, Q.; Georgakis, G. A.; Delozanne, A. L. Cryogenic Cooling Using Tunneling Structures with Sharp Energy Features. *Phys. Rev. B* **1995**, *52*, 5714–5736.
6. Williams, C. C.; Wickramasinghe, H. K. Microscopy of Chemical-Potential Variations on an Atomic Scale. *Nature* **1990**, *344*, 317–319.
7. Rettenberger, A.; Baur, C.; Lauger, K.; Hoffmann, D.; Grand, J. Y.; M?ller, R. Variation of the Thermovoltage Across a Vacuum Tunneling Barrier - Copper Islands on Ag(111). *Appl. Phys. Lett.* **1995**, *67*, 1217–1219.
8. Poler, J. C.; Zimmermann, R. M.; Cox, E. C. Scanning Thermopower Microscopy of Guanine Monolayers. *Langmuir* **1995**, *11*, 2689–2695.
9. Homoth, J.; Wenderoth, M.; Engel, K.; Druga, T.; Loth, S.; Ulbrich, R. Reconstruction of the Local Density of States in Ag(111) Surfaces Using Scanning Tunneling Potentiometry. *Phys. Rev. B* **2007**, *76*, 193407.
10. Schneider, A.; Wenderoth, M.; Engel, K. J.; Rosentreter, M. A.; Heinrich, A. J.; Ulbrich, R. G. Local Electronic Structure at Steps on Au(111) Investigated by the Thermovoltage in Scanning Tunneling Microscopy. *Appl. Phys. A: Mater. Sci. Process.* **1998**, *66*, S161–S165.
11. Grafstrom, S. Photoassisted Scanning Tunneling Microscopy. *J. Appl. Phys.* **2002**, *91*, 1717–1753.
12. Altfeder, I.; Voevodin, A. A.; Roy, A. K. Vacuum Phonon Tunneling. *Phys. Rev. Lett.* **2010**, *105*, No. 166101.
13. Menges, F.; Riel, H.; Stemmer, A.; Gotsmann, B. Quantitative Thermometry of Nanoscale Hot Spots. *Nano Lett.* **2012**, *12*, 596–601.
14. Ke, S.-H.; Yang, M.; Curtarolo, S.; Baranger, H. U. Thermopower of Molecular Junctions: an *Ab Initio* Study. *Nano Lett.* **2009**, *9*, 1011–1014.
15. Quek, S. Y.; Choi, H. J.; Louie, S. G.; Neaton, J. B. Thermopower of Amine - Gold-Linked, Aromatic Molecular Junctions From First Principles. *ACS Nano* **2011**, *5*, 551–557.
16. Widawsky, J. R.; Darancet, P.; Neaton, J. B.; Venkataraman, L. Simultaneous Determination of Conductance and Thermopower of Single Molecule Junctions. *Nano Lett.* **2012**, *12*, 354–358.
17. Lunde, A. M.; Flensberg, K. On the Mott Formula for the Thermopower of Non-Interacting Electrons in Quantum Point Contacts. *J. Phys.: Condens. Matter* **2005**, *17*, 3879–3884.
18. Markussen, T.; Jin, C.; Thygesen, K. S. Quantitatively Accurate Calculations of Conductance and Thermopower of Molecular Junctions. *Phys. Status Solidi B* **2013**, *250*, 2394–2402.
19. Pauly, F.; Viljas, J. K.; Cuevas, J. C.; Schoen, G. Density-Functional Study of Tilt-Angle and Temperature-Dependent Conductance in Biphenyl Dithiol Single-Molecule Junctions. *Phys. Rev. B* **2008**, *77*.
20. Reuter, M. G.; Harrison, R. J. Rethinking First-Principles Electron Transport Theories with Projection Operators: the Problems Caused by Partitioning the Basis Set. *J. Chem. Phys.* **2013**, *139*.
21. Hoffmann, D.; Grand, J. Y.; M?ller, R.; Rettenberger, A.; Lauger, K. Thermovoltage Across a Vacuum Barrier Investigated by Scanning-Tunneling-Microscopy - Imaging of Standing Electron Waves. *Phys. Rev. B* **1995**, *52*, 13796–13798.
22. Hoffmann, D.; Seifritz, J.; Weyers, B.; Müller, R. Thermovoltage in Scanning Tunneling Microscopy. *J. Electron Spec. Rel. Phen.* **2000**, *109*, 117–125.
23. Seifritz, J.; Wagner, T.; Weyers, B.; Müller, R. Analysis of a $SeCl_4$-Graphite Intercalate Surface by Thermovoltage Scanning Tunneling Microscopy. *Appl. Phys. Lett.* **2009**, *94*.
24. Pivetta, M.; Patthey, F.; Stengel, M.; Baldereschi, A.; Schneider, W.-D. Local Work Function Moiré Pattern on Ultrathin Ionic Films: NaCl on Ag(100). *Phys. Rev. B* **2005**, *72*, 115404.
25. Stovneng, J. A.; Lipavsky, P. Thermopower in Scanning-Tunneling-Microscope Experiments. *Phys. Rev. B* **1990**, *42*, 9214–9216.
26. Maksymovych, P. Distance Dependence of Tunneling Thermovoltage on Metal Surfaces. *J. Vac. Sci. Technol. B* **2013**, *31*, 031804.
27. Park, J.; He, G.; Feenstra, R. M.; Li, A.-P. Atomic-Scale Mapping of Thermoelectric Power on Graphene: Role of Defects and Boundaries. *Nano Lett.* **2013**, *13*, 3269–3273.
28. Volokitin, A. I.; Persson, B. N. J. Near-Field Radiative Heat Transfer and Noncontact Friction. *Rev. Mod. Phys.* **2007**, *79*, 1291–1329.
29. Zhu, X. F.; Zhang, H. F.; Williams, J. S.; Wang, R. P.; Zhang, L. D.; Wu, X. J. Low-Temperature Thermopower in Nanostructured Silver. *Appl. Phys. Lett.* **1999**, *75*, 136–138.
30. Ludoph, B.; van Ruitenbeek, J. M. Thermopower of Atomic-Size Metallic Contacts. *Phys. Rev. B* **1999**, *59*, 12290.
31. Pauly, F.; Viljas, J. K.; Cuevas, J. C. Length-Dependent Conductance and Thermopower in Single-Molecule Junctions of Dithiolated Oligophenylene Derivatives: A Density Functional Study. *Phys. Rev. B* **2008**, *78*, 035315.
32. Reinert, F.; Nicolay, G.; Schmidt, S.; Ehm, D.; Hufner, S. Direct Measurements of the L-Gap Surface States on the (111) Face of Noble Metals by Photoelectron Spectroscopy. *Phys. Rev. B* **2001**, *63*, 115415.
33. Wang, R. Y.; Feser, J. P.; Lee, J.-S.; Talapin, D. V.; Segalman, R.; Majumdar, A. Enhanced Thermopower in PbSe Nanocrystal Quantum Dot Superlattices. *Nano Lett.* **2008**, *8*, 2283–2288.
34. Heremans, J. P.; Jovovic, V.; Toberer, E. S.; Saramat, A.; Kurosaki, K.; Charoenphakdee, A.; Yamanaka, S.; Snyder, G. J. Enhancement of Thermoelectric Efficiency in PbTe by

Distortion of the Electronic Density of States. *Science* **2008**, *321*, 554–557.
35. Wang, R.-Q.; Sheng, L.; Shen, R.; Wang, B.; Xing, D. Y. Thermoelectric Effect in Single-Molecule-Magnet Junctions. *Phys. Rev. Lett.* **2010**, *105*.
36. Dubi, Y.; Di Ventra, M. Thermospin Effects in a Quantum Dot Connected to Ferromagnetic Leads. *Phys. Rev. B* **2009**, *80*, 081302.
37. Garg, A.; Rasch, D.; Shimshoni, E.; Rosch, A. Large Violation of the Wiedemann-Franz Law in Luttinger Liquids. *Phys. Rev. Lett.* **2009**, *103*, 096402.
38. Guo, S.; Zhou, G.; Tao, N. Single Molecule Conductance, Thermopower, and Transition Voltage. *Nano Lett.* **2013**, *13*, 4326–4332.
39. Pauly, F.; Viljas, J. K.; Burke, M.; Dreher, M.; Nielaba, P.; Cuevas, J. C. Molecular Dynamics Study of the Thermopower of Ag, Au, and Pt Nanocontacts. *Phys. Rev. B* **2011**, *84*, 195420.
40. Forster, F.; Nicolay, G.; Reinert, F.; Ehm, D.; Schmidt, S.; Hufner, S. Surface and Interface States on Adsorbate Covered Noble Metal Surfaces. *Surf. Sci.* **2003**, *532*, 160–165.
41. Chiang, T. C. Photoemission Studies of Quantum Well States in Thin Films. *Surf. Sci. Rep.* **2000**, *39*, 181–235.
42. Cerda, J.; Yoon, A.; Van Hove, M. A.; Sautet, P.; Salmeron M.; Somorjai, G. A. Efficient Method for the Simulation of STM Images. II. Application to Clean Rh(111) and Rh(111)+C(4 × 2)-2S. *Phys. Rev. B* **1997**, *56*, 15900–15918.
43. Soler, J. M.; Artacho, E.; Gale, J. D.; Garcia, A.; Junquera, J.; Ordejon, P.; Sanchez-Portal, D. The SIESTA Method for *Ab Initio* Order-N Materials Simulation. *J. Phys.: Condens. Mater.* **2002**, *14*, 2745–2779.
44. Rossen, E. T. R.; Flipse, C. F. J.; Cerda, J. I. Lowest Order in Inelastic Tunneling Approximation: Efficient Scheme for Simulation of Inelastic Electron Tunneling Data. *Phys. Rev. B* **2013**, *87*, 235412.
45. Perdew, J. P.; Burke, K.; Ernzerhof, M. Generalized Gradient Approximation Made Simple. *Phys. Rev. Lett.* **1996**, *77*, 3865–3868.